Comparison of Analog and Digital Transceiver Systems for MR Imaging

Article *in* Magnetic Resonance in Medical Sciences · August 2014

DOI: 10.2463/mrms.2013-0114 · Source: PubMed

3 authors, including:

Katsumi Kose
MRIsimulations Inc.
136 PUBLICATIONS **1,625** CITATIONS
SEE PROFILE

Tomoyuki Haishi
International University of Health and Welfare
87 PUBLICATIONS **874** CITATIONS
SEE PROFILE

Magn Reson Med Sci, Vol. 13, No. 4, pp. 285–291, 2014
doi:10.2463/mrms.2013-0114

TECHNICAL NOTE

Comparison of Analog and Digital Transceiver Systems for MR Imaging

Seitaro HASHIMOTO[1], Katsumi KOSE[1]*, and Tomoyuki HAISHI[2]

[1]*Institute of Applied Physics, University of Tsukuba*
1–1–1 Tennodai, Tsukuba 305–8573, Japan
[2]*MR Technology, Inc.*

(Received November 18, 2013; Accepted April 2, 2014; published online August 27, 2014)

We critically evaluated analog and digital transceivers for magnetic resonance (MR) imaging systems under identical experimental conditions to identify and compare their advantages and disadvantages. MR imaging experiments were performed using a 4.74-tesla vertical-bore superconducting magnet and a high sensitivity gradient coil probe. We acquired 3-dimensional spin echo images of a kumquat with and without using a gain-stepping scan technique to extend the dynamic range of the receiver systems. The acquired MR images clearly demonstrated nearly identical image quality for both transceiver systems, but DC and ghosting artifacts were obtained for the analog transceiver system. We therefore concluded that digital transceivers have several advantages over the analog transceivers.

Keywords: ***analog*, *digital*, *dynamic range*, *MRI*, *transceiver***

Introduction

Recent developments in digital circuits and semiconductor technology have led to the replacement of analog circuits by digital electronic circuits in magnetic resonance (MR) imaging systems. Research into digital MR imaging systems started in the late 1980s,[1–4] and the change from analog to digital systems by major whole-body MR imaging manufacturers started in the 1990s. To date, a number of digital receiver and transceiver systems for nuclear magnetic resonance (NMR) and MR imaging research have been reported,[5–9] particularly for the multiple receivers used in parallel imaging.[10–16]

The advantages of digital transceivers over analog transceivers are widely believed to include better gain balance and orthogonality between pairs of receiver channels, a wider receiver dynamic range, freedom from DC or low frequency artifacts, and better stability and reproducibility of reference phases. However, to our knowledge, no report has confirmed these advantages experimentally. We compared analog and digital transceivers developed by the same manufacturer under identical experimental conditions and confirmed several of the claimed advantages of digital transceivers over the analog transceiver.

*Corresponding author, Phone: +81-29-853-5335, Fax: +81-29-853-5205, E-mail: kose@bk.tsukuba.ac.jp

Transceiver Systems

Analog transceiver system

Figure 1(a) shows the main circuit board for the direct-conversion analog transceiver we evaluated. This transceiver was developed by MR Technology, Inc. (Tsukuba, Ibaraki, Japan) and Digital Signal Technology, Inc. (Asaka, Saitama, Japan), designed for a 202-MHz Larmor frequency, and installed in a 2U (3.5-inch height) 19-inch rack-mounting unit.

Figure 1(b) shows a block schematic diagram for the analog transceiver system. The transceiver was controlled by an MR imaging pulse programmer,[17] developed via a digital signal processor (DSP) board (DSP6031, MTT Corp., Kobe, Japan) implemented using a DSP chip (TMS320C31, Texas Instruments, Houston, TX, USA) running at 40 MHz, and interfaced with a host PC. The host PC included a Core 2 Duo microprocessor (Intel, Santa Clara, CA, USA) with a clock frequency of 2.13 GHz and 4 GB of random access memory (RAM), running under the Windows XP operating system (Microsoft, Redmond, WA, USA).

Radiofrequency (RF) pulses were generated us-

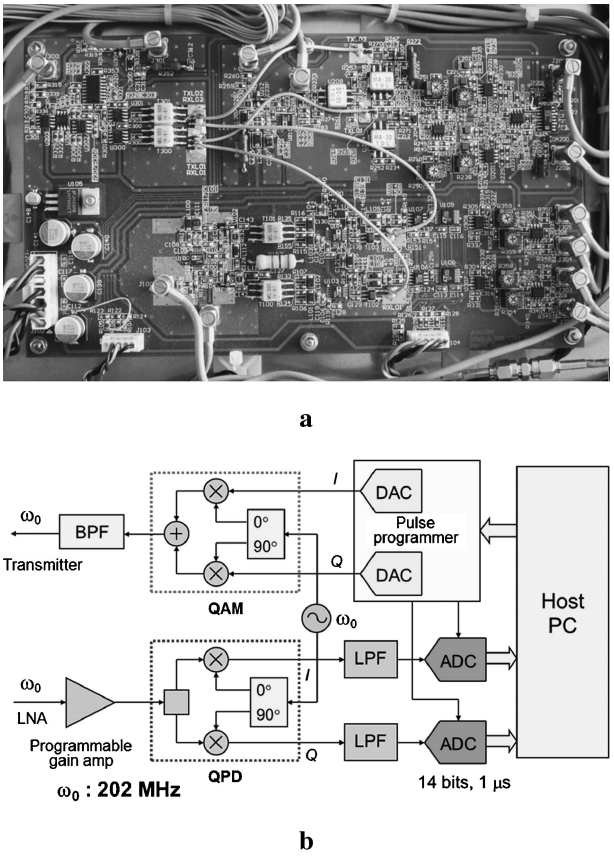

Fig. 1. (**a**) Main circuit board. (**b**) Block diagram for the analog transceiver.

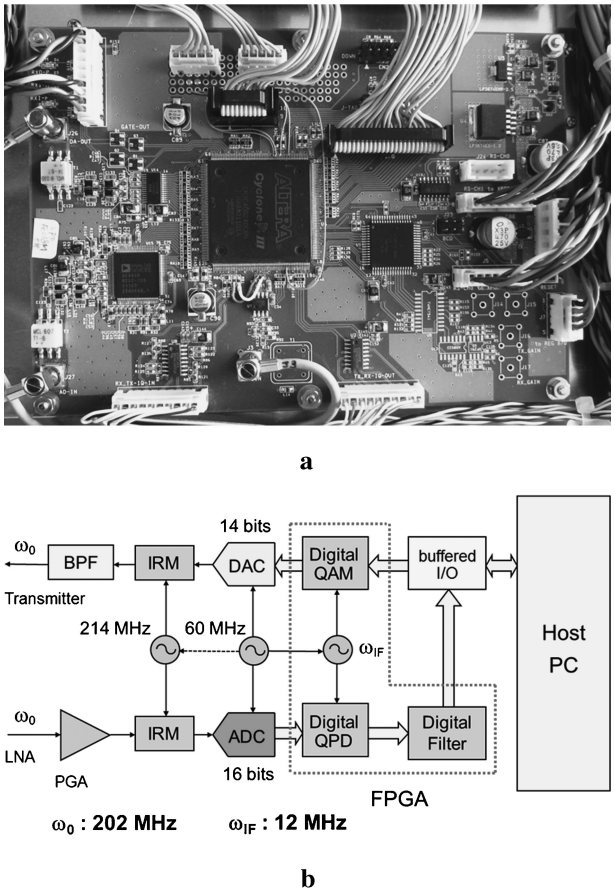

Fig. 2. (**a**) Main circuit board. (**b**) Block diagram for the digital transceiver.

ing a quadrature amplitude modulator (QAM) for which waveforms were generated by 16-bit digital-to-analog (DA) converters controlled by the pulse programmer. The sampling interval for the in-phase and quadrature-phase waveforms was 8 μs. A coherent RF signal source (404 MHz) for twice the Larmor frequency was generated by a direct digital synthesizer (MG3641A, ANRITSU Inc., Atsugi, Japan).

The 202-MHz NMR signal detected by an RF probe and amplified with a low noise amplifier (LNA) was further amplified using a programmable gain amplifier in the transceiver. The amplified NMR signal was directly demodulated with a quadrature phase-sensitive detector (QPD) using the 404-MHz reference signal. The QPD contained 2 active mixers (AD8343, Analog Devices, Norwood, MA, USA). The detected in-phase and quadrature-phase baseband signals were filtered using monolithic digitally controlled 8th-order low pass filters (LTC1565, Linear Technology Corp., Milpitas, CA, USA).

The filtered 2-channel signals were digitally sampled simultaneously using a 2-channel analog-to-digital converter (ADC) board (PC-414G3, DATEL, USA) interfaced with the host PC via an industry standard architecture bus. The resolution of the ADC was 14 bits and the minimum sampling interval, one μs. Because the sampling clock was generated by an 8-MHz internal base clock and used in the external trigger mode, a skew delay (125 ns maximum) was included for the signal sampling.

Digital transceiver system

Figure 2(a) shows the main circuit board for the digital transceiver we evaluated. This transceiver was also developed by MR Technology, Inc. and Digital Signal Technology, Inc. Because the digital transceiver was originally designed for Larmor frequencies lower than 15 MHz, a frequency converter (up-down converter) unit was developed that converted between a 202-MHz RF signal and a 12-MHz intermediate frequency signal in either direction. The whole transceiver system, including the frequency converter unit, was installed in a 2U 19-inch rack-mounting unit.

Figure 2(b) shows a block schematic diagram of the digital transceiver system. The transceiver was controlled by a PC-based pulse programmer[18] developed using a high speed digital interface board

with a large buffer memory (NI-6534, National Instruments, Austin, TX, USA). The host PC included a Core i7 microprocessor (Intel) and 16 GB of RAM running under the Windows 7 operating system (Microsoft).

The QAM, QPD, and digital filters were implemented as logic circuits using a field-programmable gate array (FPGA) (Cyclone III, ALTERA, San Jose, CA, USA) and a 60-MHz clock generated by a phase-locked loop synthesizer unit (EPLO-60MF, Digital Signal Technology, Inc.) with a built-in temperature-compensated crystal oscillator module.

The in-phase and quadrature-phase waveforms of the RF pulses were supplied as 16-bit digital datasets by the PC-MR imaging pulse programmer. The sampling interval for the RF pulse waveforms was one μs. The intermediate frequency (12 MHz) was generated by a numerical oscillator implemented in the FPGA. The numerically modulated 12-MHz RF pulse datasets were converted to analog RF pulses using a 14-bit DA converter (DAC904, Burr Brown, Tucson, AZ, USA) with the 60-MHz clock signal identical to that supplied to the FPGA and up-converted to 202-MHz RF pulses using a 214-MHz reference signal.

The 202-MHz NMR signal detected by the RF coil and amplified with an LNA was further amplified using a programmable gain amplifier in the transceiver. The amplified NMR signal was converted to a 12-MHz NMR signal using the down-converter unit and the 214-MHz reference signal. The 12-MHz NMR signal was digitally sampled using a 16-bit ADC (AD9460-105, Analog Devices) with the 60-MHz clock. The sampled NMR signal datasets were digitally demodulated using the QPD circuit, filtered using a cascaded integrator-comb filter to a signal with a one-MHz cutoff frequency, and further filtered using a finite impulse response (FIR) filter with a 50-kHz cutoff frequency. The digitally filtered NMR signal datasets with 16-bit resolution were transferred from the transceiver to the host PC every one μs via the high speed digital interface board already described. The data transfer rate from the transceiver to the host PC was 128 Mbit/s.

Experiments

Figure 3 shows the MR imaging system used to evaluate the analog and digital transceiver systems, which included a 4.74-tesla vertical-bore superconducting magnet (diameter of the room-temperature bore, 88.3 mm, Oxford Instruments, Abingdon, UK), a home-built gradient-coil probe with a solenoid RF coil (40-mm inner diameter, 60-mm length),[19] 2 wideband low noise preamplifiers (N141-305AA, 5 ~ 500 MHz, 30 dB gain, Thamway, Fuji, Japan), the analog and digital transceivers described above, a wideband RF transmitter (300 W, M3205A, American Microwave Technology, Brea, CA USA), a 3-channel gradient driver (±20 V, ±10 A), and the 2 host PCs described above.

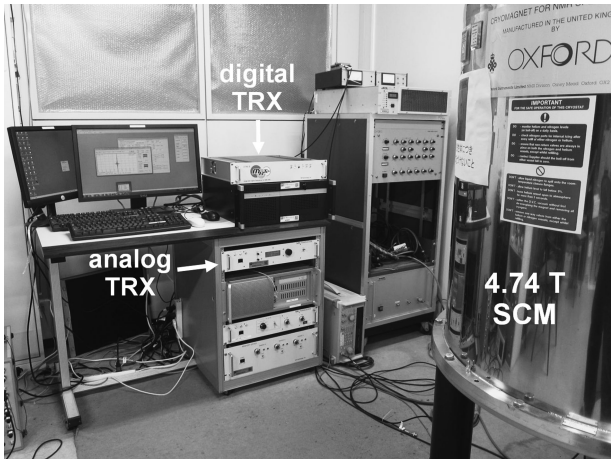

Fig. 3. Overview of the magnetic resonance imaging system used in the experiments.

The efficiencies of the planar gradient coils were 7.0 mT/m/A for the Gx, 5.4 for the Gy, and 9.2 for the Gz coils. The RF coil was a 6-turn solenoid coil wound with a polyurethane-coated Cu wire of 2.0-mm diameter divided by five 5.1-pF nonmagnetic chip capacitors (Voltronics, Salisbury, MD, USA).

MR images of a kumquat (diameter ~ 35 mm) were acquired with a 3-dimensional (3D) spin-echo (SE) sequence using both transceiver systems. The parameters of the pulse sequence were: field of view, 40.96-mm cube; image matrix, 512 (readout) × 512 × 64; repetition time, 800 ms; spin echo time, 20 ms; number of excitations, one; and total imaging time, 7.3 hours. For the analog receiver, the sampling frequency of the detected signal was 50 kHz (20-μs dwell time), and 512 complex (2-channel) points were sampled for each readout signal. For the digital receiver, the recording frequency of the detected signal was 200 kHz (5-μs dwell time), and 2048 complex points were recorded for each readout signal to avoid noise aliasing.

To extend the dynamic range of the receiver systems, we used a gain-stepping scan technique[20–22] for both analog and digital transceivers and acquired MR imaging signal data with a low gain (0 dB) in the central region (512 [readout] × 32 × 32) of the k-space and with a high gain (+30 dB) in the region of high spatial frequency of the k-space. In practice, the gain-stepping scan was performed by 2 separate scans with different gain settings using a

passive variable attenuator inserted between the preamplifier and receivers. We therefore call a scan with gain stepping "dual scan" and a scan without gain stepping "single scan." Because the data acquisition time for the scan in the central region was only about 13.7 minutes, the data acquisition time was only about 3% longer for the dual scan than the single scan. For the dual scan, image reconstruction was performed after synthesis of the MR imaging signal data from the 2 datasets acquired in the 2 regions of the k-space.

For image reconstruction, we used 3D Fourier transforms that involved $512 \times 512 \times 64$ points for the analog and $2048 \times 512 \times 64$ points for the digital receivers.

Results

Relation between the gain-stepping scan and image quality

Figures 4(a) through (d) show identical cross sections selected from 3D image datasets acquired with the 3D SE sequence using the analog and digital transceiver systems. Figures 4(a) and (b) were acquired using the analog transceiver without and with the 30 dB gain-stepping scan. Figures 4(c) and (d) were acquired using the digital transceiver without and with the gain-stepping scan.

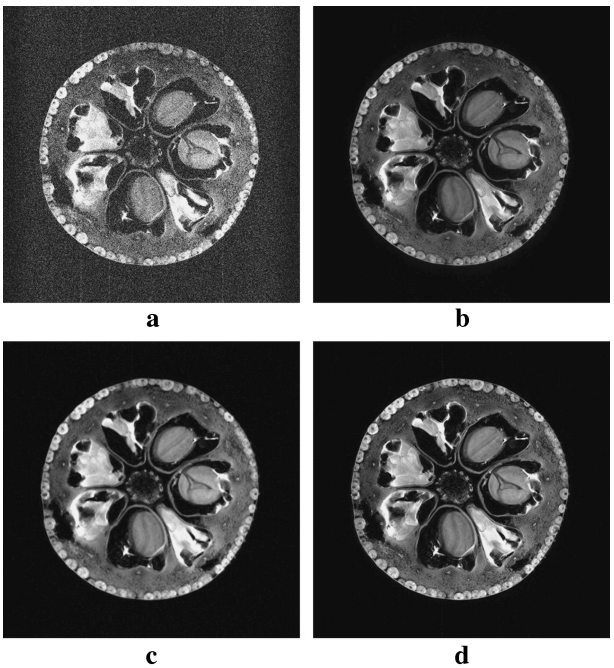

Fig. 4. (**a**, **b**) Two-dimensional (2D) cross sections selected from 3D image datasets acquired with the analog transceiver. (**c**, **d**) Two-dimensional cross sections selected from 3D image datasets acquired with the digital transceiver. (**a**, **c**) Acquired without the gain-stepping scan. (**b**, **d**) Acquired with the gain-stepping scan and showing similar image quality.

Figures 4(a) and (b) clearly show the signal-to-noise ratio (SNR) of the cross-sectional image is drastically improved using the gain-stepping scan for the analog transceiver. Figures 4(c) and (d) clearly show improved spatial resolution using the gain-stepping scan for the digital transceiver, although the SNRs of the cross-sectional images seem nearly identical. In both cases, the gain-stepping scan achieved similarly high image quality for both SNR and spatial resolution (Figs. 4[b], [d]).

Figure 5 shows the relative average signal power in the k-space plotted against the wave number of the MR signal of the kumquat, which we call the "k-power plot,"[22–24] obtained with and without the gain-stepping scan for the analog and digital transceivers.

For the analog transceiver, the signal dynamic range for the single scan is about 64 dB and the noise floor (probably caused by the internal noise of the analog receiver) is clearly observed as the flat part of the graph at −64 dBr. Use of the dual scan permits extension of the dynamic range to about 80 dB, and the high frequency signal components are properly sampled.

For the digital transceiver, the dynamic range seems larger for the single scan than the dual scan, which is the opposite of that for the analog receiver. The k-power plot for the dual scan in Fig. 5(b) is almost identical to that for the analog receiver in Fig. 5(a), which corresponds with nearly identical image quality (Figs. 4[b], [d]).

Artifacts and noise

Figures 6(a) and (b) are enlarged central parts of Figs. 4(b) and (d). The presence of the DC artifact in the image acquired with the analog receiver is clearly observed. However, no other low frequency noise is observed.

Figures 6(c) and (d) are cross-sectional images for which display-window levels are expanded to demonstrate the background noise and artifacts. The image acquired with the analog transceiver shows low spatial-frequency distortion in both the readout and phase-encoding directions and ghosting artifacts in the phase-encoding direction. The image acquired by the digital transceiver shows only random or white-spectrum background noise except for a small RF leak caused by the RF converter unit.

Figures 6(e) and (f) show the regions in which signal or noise amplitudes were calculated to evaluate the images shown in Figs. 6(c) and (d). For the analog receiver, the noise amplitude in the phase-encoding direction averaged over Region A is 4.1%, and that in the readout direction averaged

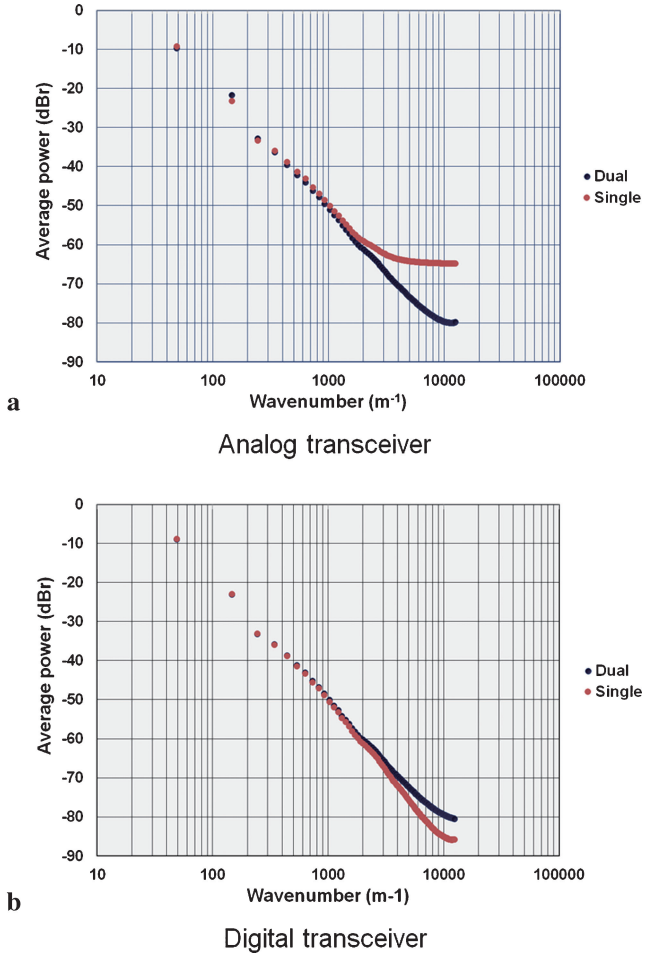

Fig. 5. (**a**) Average relative power of the nuclear magnetic resonance (NMR) signal plotted against the wave number in the k-space (k-power plot), acquired using the analog transceiver with and without the gain-stepping scan. The dynamic range of the NMR signal is extended by the dual scan. (**b**) The k-power plot acquired using the digital transceiver with and without the gain-stepping scan. The dynamic range of the NMR signal seems to be reduced by the dual scan.

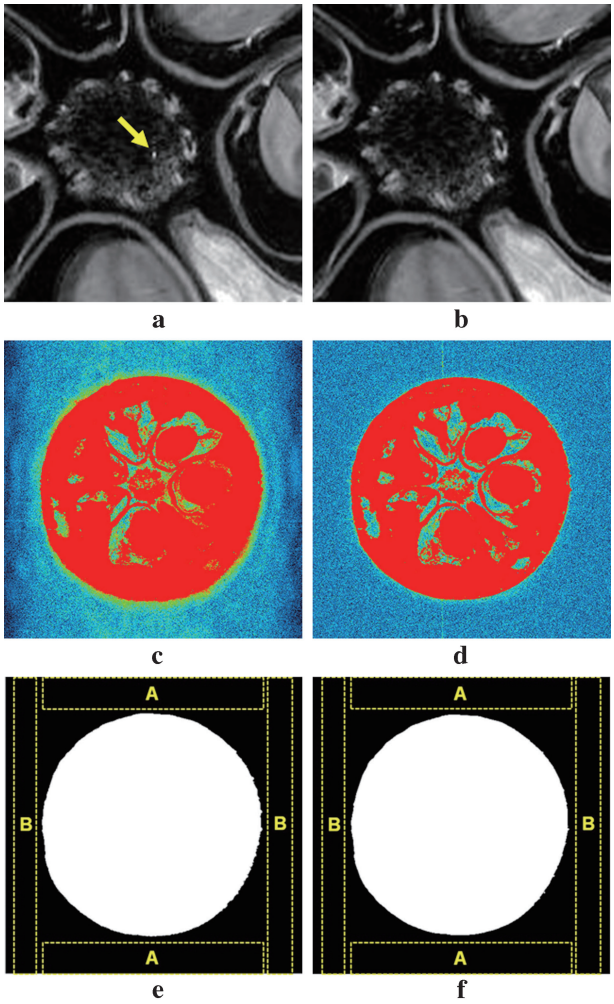

Fig. 6. (**a**, **b**) Zoomed images of Figs. 4b and d. (**c**, **d**) The images in Figs. 4b and d with extended window level. (**e**, **f**) Regions used for noise evaluation in Figs. 4b and d.

over Region B is 2.6% of the signal intensity averaged over the segmented central region. For the digital receiver, the corresponding values are 3.2% (phase-encoding direction over Region A) and 3.3% (readout direction over Region B). These values show that the background noise for the images acquired with the analog transceiver is anisotropic, whereas that for the digital transceiver is isotropic.

Discussion

As we mentioned in the Introduction, the advantages of the digital transceiver over the analog transceiver are widely believed to include better gain balance and orthogonality between the 2 receiver channels, a wider receiver dynamic range, freedom from DC or low frequency artifacts, and better stability and reproducibility of reference phases. Here we discuss these issues in the context of our experimental results.

Gain balance and orthogonality between receiver channels

If the gain balance and orthogonality between the 2 receiver channels are not well established in the analog receiver, a symmetric ghost artifact is observed in MR images. However, we observed no clear symmetric ghost artifact (Fig. 4[b]). This is because the SNR of the MR image was not high (around 50), and gain balance and orthogonality were well achieved by fine-tuning the receiver channels of the analog receiver used in the experiments. As shown in Fig. 6(d), we observed no symmetric ghost for the digital receiver.

Receiver dynamic range

The SNR of the digitally sampled full-scale sinusoidal wave is well known to be $SNR = 6.02N + 1.76 + 10\log\left(\frac{f_s}{2B}\right) dB$, where N is the bit resolution, f_s, the sampling frequency of the ADC, and B, the bandwidth of the signal.[5] In our experimental conditions, because $N = 16$, $f_s = 60$ MHz, and $B = 50$ kHz, the SNR for the full-scale sinusoidal wave is about 126 dB if there is no analog noise in the ADC. From the datasheet of the AD9640-105 used in our digital receiver, the SNR for an input of 10 MHz is about 76 dB, −22 dB down from the ideal value (98 dB). Therefore, an SNR of about 104 dB can be expected for the full-scale sinusoidal signal in the digital receiver.

In the digital receiver, the acquired NMR signal was digitally demodulated and decimated to generate 2-channel 16-bit signal data every one μs. These output digital data correspond to 106-dB SNR for the full-scale sinusoidal signal, if the 50-kHz signal bandwidth is used. Therefore, the bit resolution and data output rate (one μs) for the output data was sufficient for the RF sampling at 60 MHz. However, as shown in the results for the single and dual scans using the digital receiver, great care in setting the signal amplitude is indispensable.

The k-power plot for the analog and digital receivers demonstrates the dynamic range of the MR imaging signal acquired from the kumquat was about 80 dB. Correct digital sampling of this signal required more than 15-bit (±14-bit) resolution. However, in the single-scan experiment using the digital receiver, the maximum number of digital signals was 5667, which was caused by an incorrect amplitude setting. Figures 4(c) and 5(b) demonstrate the loss of the components of high spatial frequency by inadequate gain setting for the digital transceiver because the amplitudes of those components are generally very small ($<\sim 1/5000$ of the amplitude of the echo peak) and were rounded to zero values. However, because the dual scan technique "recovered" the components of high spatial frequency, a correct MR image was obtained (Fig. 4[d]).

To date, though MR signals with a dynamic range greater than 100 dB have been reported for some extreme cases, such as in high field whole mouse imaging,[22] several publications have reported the dynamic ranges of most MR signals for clinical imaging to be less than about 90 dB.[20,24] Therefore, although a correct gain setting is indispensable, a 16-bit digital resolution is sufficient for most MR imaging.

DC and low frequency artifacts

Figures 6(a) and (b) show that the DC artifact is observed only in the image acquired via the analog receiver. However, we observed no low frequency artifacts, such as those caused by power lines or 1/f noise, because the analog receiver was well designed and manufactured. Because software-based offset correction can eliminate DC noise, DC and low frequency artifacts cannot be seen as disadvantages for our analog transceiver.

Phase reproducibility and/or stability

As described in our Results, background noise was greater in the phase-encoding direction (4.1%) than the readout direction (2.6%) for the image acquired via the analog transceiver, whereas the background noise for the image acquired via the digital transceiver was isotropic. The anisotropy of the background noise for the analog transceiver is considered to be caused by instability of the transmitter and/or receiver phases because noise in the reference signal directly affects the phase of the RF pulse and the detected NMR signal. On the other hand, we observed no phase instability for the digital transceiver, as indicated by the isotropic property of the background noise.

Data storage and image processing time

Because the bandwidth of the FIR filter in the digital transceiver was (temporarily) fixed at 50 kHz and its cutoff character was limited, oversampling was required for the digital receiver. Therefore, the data storage and image processing time for the digital transceiver were 2 to 4 times those for the analog transceiver. This issue may be the single disadvantage of the digital transceiver when compared with the analog transceiver.

Conclusion

We critically compared analog and digital transceivers for MR imaging under identical experimental conditions and confirmed that the DC artifact and instability of the MR imaging signal phase for the analog receiver were not present for the digital receiver. Although the dynamic range of the digital receiver exceeded that of the analog receiver, a correct gain setting was essential to utilize the wide dynamic range of the digital receiver.

In conclusion, the digital transceiver has several advantages over the analog transceiver, but a careful gain setting is indispensable to achieve the benefit of the wide receiver dynamic range.

Acknowledgement

We thank Mr. Masaru Aoki at Digital Signal Technology, Inc. for the development and construction of the analog and digital transceivers.

References

1. Proska R. A fully digital spectrometer for low field MR imaging systems. Abstract VII SMRM Meeting, San Francisco, 1988; 266.
2. Mehlkopf AF, den Boef JH. A novel, simple and high performance MRI/MRS transmit/receive system. Abstract VII SMRM Meeting, San Francisco, 1988; 857.
3. Holland GN, Blakeley DM, Stauber JR, Flugan D, Denison KS. The design and comparative evaluation of a digital transmitter/receiver (DTR) for MR imaging. Abstract VIII SMRM Meeting, Amsterdam, 1989; 182.
4. Stormont RS, Noonan PJ, Pelc NJ, et al. A new transceiver for MR imaging and spectroscopy. Abstract VIII SMRM Meeting, Amsterdam, 1989; 962.
5. Villa M, Tian F, Confrancesco P, Halamek J, Kasal M. High-resolution digital quadrature detection. Rev Sci Instrum 1996; 67:2123.
6. Michal CA, Broughton K, Hansen E. A high performance digital receiver for home-built nuclear magnetic resonance spectrometers. Rev Sci Instrum 2002; 73:453.
7. Jie S, Qin X, Yang L, Gengying L. Home-built magnetic resonance imaging system (0.3 T) with a complete digital spectrometer. Rev Sci Instrum 2005; 76:105101.
8. Takeda K. A highly integrated FPGA-based nuclear magnetic resonance spectrometer. Rev Sci Instrum 2007; 78:033103.
9. Stang P, Conolly SM, Santos JM, Pauly JM, Scott GC. A Scalable MR Console Using USB. IEEE Trans Med Imaging 2012; 31:370.
10. Bodurka J, Ledden PJ, van Gelderen P, et al. Scalable multichannel MRI data acquisition system. Magn Reson Med 2004; 51:165–171.
11. Perez P, Santos A. Undersampling to acquire nuclear magnetic resonance images. Med Engin Phys 2004; 26:523.
12. Bollenbeck J, Vester M, Oppelt R, Kroeckel H, Schnell W. A high performance multi-channel RF receiver for magnetic resonance imaging systems. Proc Intl Soc Mag Reson Med 2005; 860.
13. Giovannetti G, Hartwig V, Viti V, et al. Application of Undersampling Technique for the Design of an NMR Signals Digital Receiver. Concepts Magn Reson 2006; Part B 29B:107.
14. Sipilä P, Schulte RF, Wachutka G, Wiesinger F. Digital multiband receiver for magnetic resonance. Concepts Magn Reson 2009; Part B 35B:210.
15. Possanzini C, van Liere P, Roeven H, et al. Scalability and channel independency of the digital broadband dStream architecture. Proc Intl Soc Magn Reson Med 2011; 1863.
16. Tang W, Sun H, Wang W. A digital receiver module with direct data acquisition for magnetic resonance imaging systems. Rev Sci Instrum 2012; 83:104701.
17. Kose K, Haishi T. evelopment of a flexible pulse programmer for MRI using a commercial digital signal processor board. In: Blumler P, Blumich B, Botto R, Fukushima E, eds. Spatially resolved magnetic resonance. Weinheim, Germany: Wiley-VCH, 1998; 703.
18. Hashimoto S, Kose K, Haishi T. Development of a pulse programmer for magnetic resonance imaging using a personal computer and a high-speed digital input–output board. Rev Sci Instrum 2012; 83: 053702.
19. Horiga M, Ishizawa K, Kose K. Development of gradient coil probes for vertical wide bore superconducting magnets with solenoid RF coils and optimized planar gradient coils, Proc Intl Soc Magn Reson Med 2013: 2712.
20. Kose K, Endoh K, Inouye T. Nonlinear amplitude in magnetic resonance imaging: quantization noise reduction and data memory saving. IEEE Aerosp Electron Syst Mag 1990; 5:27.
21. Elliott MA, Insko EK, Greenman RL, Leigh JS. Improved resolution and signal-to-noise ratio in MRI via enhanced signal digitization. J Magn Reson 1998; 130:300–304.
22. Behin R, Bishop J, Henkelman RM. Dynamic range requirements for MRI. Concepts Magn Reson 2005; Part B 26B:28.
23. Fuderer M. The information content of MR images. IEEE Trans Med Imaging 1988; 7:368.
24. Otake Y, Kose K, Haishi T. A solution to the dynamic range problem in MRI using a parallel image acquisition. Concepts Magn Reson 2006; Part B 29B:161.
25. Gabr RE, Schär M, Edelstein AD, Kraitchman DL, Bottomley PA, Edelstein WA. MRI dynamic range and its compatibility with signal transmission media. J Magn Reson 2009; 198:137–145.